

# Model-free kinetics analysis of nanocrystalline HZSM-5 catalyzed pyrolysis of polypropylene (PP)

B. Saha, P. Karthik Reddy, Aie Cheng King Chowlu, A.K. Ghoshal\*

*Department of Chemical Engineering, Indian Institute of Technology Guwahati, Guwahati 39, Assam, India*

Received 6 August 2007; received in revised form 30 November 2007; accepted 9 December 2007

Available online 17 December 2007

## Abstract

Catalytic decomposition behaviour polypropylene (PP) is studied over nanocrystalline HZSM-5 (n-HZSM-5) catalyst. The catalyst is synthesized using the standard procedure reported in the literature. The catalyst is characterized by X-ray diffraction, scanning electron microscopy and nitrogen adsorption studies. Catalytic decomposition of PP is studied at five different heating rates. Vyazovkin model-free kinetic analysis is carried out to understand the variation of activation energy,  $E_\alpha$  with conversion,  $\alpha$ . Result shows that n-HZSM-5 catalyst has excellent catalytic effect in terms of reduction in activation energy due to its high external surface area ( $364 \text{ m}^2 \text{ g}^{-1}$ ) due to its nanometric dimensions. Presence of the catalyst significantly reduces the maximum decomposition temperature,  $T_m$  of the PP sample and the optimum catalyst percentage is around 50 wt%, where the reduction in  $T_m$  is around  $161^\circ\text{C}$ . Constant pattern behaviour in the thermogravimetric (TG) and derivative thermogravimetric (DTG) indicates existence of similar reaction mechanism. Model-free kinetic analysis indicates that  $E_\alpha$  decreases slowly and continuously with  $\alpha$  after  $\alpha \geq 0.1$ . The microporous and mesoporous catalytic activities of the different catalysts control the variation of  $E_\alpha$  with  $\alpha$  at higher values of  $\alpha$ .

© 2007 Elsevier B.V. All rights reserved.

**Keywords:** Activation energy; Catalytic decomposition; Model-free kinetic analysis; n-HZSM-5; Polypropylene

## 1. Introduction

Polypropylene (PP) has got immense utilization both in household and in industrial applications due to its lightness, rigidity, tightness, heat resistance, chemical resistance and high surface gloss. PP represents about 22 wt% of the demand for thermoplastics in the world [1]. In our recent papers, we reported model-free kinetic analysis of noncatalytic pyrolysis of plastics such as polyethylene terephthalate (PET) [2], polyethylene (PE) [3] and PP [4]. Through these papers we have shown the variations of activation energy with conversion in case of nonisothermal as well as isothermal pyrolysis of these plastic materials. We also reported, in another publication [5], that model-free coupled with model-fitting technique is a suitable approach to find out the reliable and optimum kinetics triplet (activation energy, pre-exponential factor, and reaction order) for

pyrolytic degradation of the plastic materials. In this approach, information about the reaction mechanism (in terms of different steps) and the initial guess values for the kinetics triplet are successfully used in the model-fitting method of analysis. Recently, we reported (probably the first time) in case of catalytic decomposition of PP over Al-MCM-41 catalyst that model-free approach helps identifying the steps involved during catalytic pyrolysis [4]. Thus, through this paper [4] we demonstrated the importance and advantages of model-free kinetic analysis technique during catalytic decomposition, where reaction mechanism may change drastically with type and concentration of catalyst. In addition to the above, literature reports suggest that catalytic degradation kinetics of PP have been studied so far over catalysts such as silica gel, silica–magnesia, silica–titania, mordenite and silica–alumina [6]; BEA, ZSM-5 and MOR [7]; and over ZSM-5 and ZSM-12 catalysts [1,8]. Several researchers also reported catalytic decomposition of plastics particularly LDPE and HDPE over nanocrystalline HZSM-5 (n-HZSM-5) [9–11], a promising catalyst that has high surface area, shows high reduction of maximum decomposition temperature ( $T_m$ ) and produces mainly gaseous products.

\* Corresponding author. Tel.: +91 361 2582251;

fax: +91 361 2582291/2690762.

E-mail address: [aloke@iitg.ernet.in](mailto:aloke@iitg.ernet.in) (A.K. Ghoshal).

But to the best of our knowledge, catalytic decomposition of PP over n-HZSM-5 with its kinetics analysis is not reported yet.

In this paper, we report the effect of our laboratory synthesized catalyst n-HZSM-5 on PP decomposition. We employed the Vyazovkin model-free approach [12–14] to understand the variation of activation energy with conversion and to understand the possible reaction steps involved during this degradation. We also compared the performance of our laboratory synthesized catalyst (n-HZSM-5) for such degradation of PP with that of different other catalysts as reported in the literatures.

## 2. Experimental

### 2.1. Polymer materials

The catalytic and noncatalytic nonisothermal decompositions were carried out for PP (polypropylene homopolymer (PPHP), trade name: Koylene ADL, Grade AS030N) supplied by Indian Petrochemicals Corporation Limited, Vadodara, India with melt flow index 3.0.

### 2.2. Synthesis of n-HZSM-5

Nanocrystalline HZSM-5 catalyst was prepared by using the procedure of hydrothermal crystallization of clear supersaturated homogeneous synthesis described in literature [15,16]. Aluminum isopropoxide (>98%, Acros Organics, India) was first added to measured amount of 20% aqueous solution of tetra-propylammonium hydroxide (TPAOH, 40 wt% Merck, India). Resulting solution was stirred at 0 °C till a clear solution is obtained. Then appropriate amount of tetraethoxysilane (TEOS (98%), Merck, Germany) ( $\text{SiO}_2/\text{Al}_2\text{O}_3 = 60$ ) was added. The solution was further stirred at room temperature for several hours in order to hydrolyze TEOS completely. Then it was heated at 80 °C for 1–1.5 h to remove water and alcohols. The concentrated solution was transferred to Teflon-lined stainless steel autoclave, where it was crystallized by thermal treatment under autogenous pressure at 170 °C for about 72 h. The solid product was separated by filtration and washed several times with water. The washed sample was dried overnight at a temperature of 383 K followed by calcination in air at 550 °C for 8–9 h maintaining a heating rate of 2 K min<sup>-1</sup>.

### 2.3. Catalysts characterization

The catalysts was characterized by X-ray diffraction (XRD) analysis using Bruker AXS instrument using high angle XRD ranging 2–50°, Cu K $\alpha$  radiation (40 kV, 40 mA) with step size of 0.05° (2 $\theta$ ) and time of 0.5 s per step. Scanning electron microscope (SEM) micrograph (make: LEO, model: 1430VP) was taken to learn about its morphology. Nitrogen adsorption isotherm at 77 K was determined on SA 3100 surface analyzer from Beckman Coulter using helium (for dead space calibration) and nitrogen. The catalyst samples were out gassed for 3 h at 300 °C under nitrogen flow.

### 2.4. Thermal and catalytic decomposition experiments for PP

Nonisothermal or dynamic thermogravimetry experiments were carried out in a TGA instrument of Mettler TOLEDO with model no. TGA/SDTA 851<sup>e</sup> under nitrogen environment for a range of temperature 303–875 K. Nitrogen flow rate was maintained at 40–50 ml min<sup>-1</sup> according to the specification of the equipment. All samples, shredded into very small pieces (mesh size of –40/60), were directly fed to the TGA instrument. Thermal decomposition experiments were carried out in dynamic condition at different heating rates of 5, 10, 15, 20 and 25 K min<sup>-1</sup>. Platinum crucible (150  $\mu$ l) was used as sample holder. The experiments were repeated three times at a heating rate of 10 K min<sup>-1</sup>, to confirm the repeatability and authenticity of the generated data for all cases. The deviations observed are very little. However, the deviations are reported in terms of average relative deviation,

$$\text{ARD}(\%) = \frac{100}{N} \sum_{i=1}^N \left| \frac{x_i^{\text{exp}} - x_{\text{av},i}}{x_{\text{av},i}} \right|$$

where  $x_i^{\text{exp}}$  and  $x_{\text{av},i}$  are the experimental values of the variables (temperature and normalized mass) and average values of the variables, respectively;  $i$  is the number of data points for each experiment. Results show that ARD% are 0.005–0.019 (for temperature), 0.041–0.1579 (for mass). Experimental conditions for TGA studies are given in Table 1. Further details can be seen in our recent publications [2–5,17–19]. Catalytic decomposition experiments were carried out with different percentage of n-HZSM-5 catalysts (Table 2) at 10 K min<sup>-1</sup> for PP. The optimum catalyst percentage was found around 50 wt%

Table 1  
Nonisothermal experimental conditions for TGA studies

Sample	Nonisothermal experiments				
	Initial mass (mg)	Heating rate (K min <sup>-1</sup> )	Temperature range (K)	% Residue	$T_{W_0}/T_d/T_m/T_{W_\infty}$ (K)
PP	19.77	5	303–873	1.49	533.6/596.9/706.8/773.9
	20.32	10	303–873	0.88	526.9/670.0/723.1/749.8
	20.67	15	303–873	0.51	527.8/684.6/731.4/777.6
	19.78	20	303–873	0.73	527.5/684.8/736.8/770.2
	19.41	25	303–873	0.70	527.1/696.6/742.9/785.7

Table 2  
Experimental conditions for TGA studies using different percentages of catalyst

Catalyst	Catalyst percentage	Total initial mass (mg)	$T_m$ (K)
n-	10	14.54	644.8
HZSM-	20	13.24	604.8
5 + PP	30	13.99	591.4
	40	13.18	572.2
	50	13.46	561.6
	60	13.5	561.1

n-HZSM-5 on PP after which reduction in  $T_m$  with increase in catalyst percentage was not so significant. Further catalytic decomposition experiments were conducted using 50 wt% n-HZSM-5 on PP at different heating rates of 5, 10, 15, 20, and 25 K min<sup>-1</sup>. The experimental conditions are summarized in Table 3.

### 3. Kinetics analysis

The kinetics model equation combined with the Arrhenius approach of the temperature function of reaction rate constant is expressed as

$$\frac{d\alpha}{dt} = k_0 \exp\left(\frac{-E_\alpha}{RT}\right) f(\alpha) \quad (1)$$

where  $t$  is time (min);  $T$  the temperature (K);  $\alpha$  the conversion of reaction  $(W_0 - W)/(W_0 - W_\infty)$ ,  $W_0$  the initial weight of the sample (mg),  $W$  the sample weight (mg) at any temperature  $T$ ,  $W_\infty$  the final sample weight (mg);  $d\alpha/dt$  the rate of reaction (min<sup>-1</sup>);  $f(\alpha)$  the reaction model;  $k_0$  the pre-exponential factor (K<sup>-1</sup>);  $E_\alpha$  the activation energy (kJ mol<sup>-1</sup>) are the Arrhenius parameters;  $R$  is the gas constant (kJ mol<sup>-1</sup> K<sup>-1</sup>). At a constant heating rate under nonisothermal conditions the explicit temperature time dependence in Eq. (1) is eliminated through the trivial transformation:

$$\beta \frac{d\alpha}{dT} = k_0 \exp\left(\frac{-E_\alpha}{RT}\right) f(\alpha) \quad (2)$$

where  $\beta = dT/dt$  is the heating rate (K min<sup>-1</sup>) and  $d\alpha/dT$  is rate of reaction (K<sup>-1</sup>).

For a given conversion and a set of  $n$  experiments carried out at different heating rates  $\beta_i$  ( $i = 1, \dots, n$ ). The activation energy ( $E_\alpha$ ) can be determined at any particular value of  $\alpha$  by finding the value of  $E_\alpha$  for which the objective function  $\Omega(E_\alpha)$  [12–14]

is minimized, where

$$\Omega(E_\alpha) = \sum_{i=1}^n \sum_{j \neq i}^n \frac{I(E_\alpha, T_{\alpha,i}) \beta_j}{I(E_\alpha, T_{\alpha,j}) \beta_i} \quad (3)$$

Using experimental values of  $T_\alpha$  and  $\beta$  and minimizing the function  $\Omega(E_\alpha)$ , the value of the  $E_\alpha$  is obtained at a given conversion. The objective function,  $\Omega(E_\alpha)$  minimization is done by numerical method in MATLAB using ‘medium-scale: Quasi-Newton line search’ algorithm [20]. The ‘fminunc’ function for unconstrained problem is applied for the optimization [19], where

$$I(E_\alpha, T_{\alpha i}) = \int_0^{T_{\alpha i}} \exp\left(\frac{-E_\alpha}{RT}\right) dT \quad (4)$$

The temperature integral is evaluated by direct numerical integration, where the temperature integral takes the form:

$$\begin{aligned} I(E_\alpha, T_{\alpha i}) &= \int_0^{T_{\alpha i}} \exp\left(\frac{-E_\alpha}{RT}\right) dT \\ &= \frac{E_\alpha}{R} \left[ \frac{\exp(-u)}{u} - Ei(u) \right] \end{aligned} \quad (5)$$

where  $u = E_\alpha/RT$  and  $Ei(u) = \int_u^\infty \exp(-u)/u du$ .

Detail development of Eq. (5), numerical procedure and algorithms for model-free technique are discussed in our recent publication [3].

## 4. Results and discussion

### 4.1. Characterization of n-HZSM-5 catalysts

The XRD pattern of n-HZSM-5 catalyst (Fig. 1) clearly shows the presence of amorphous phase. A broad bottom reflection placed at  $2\theta \sim 20$ – $23^\circ$  corresponding to the possible contribution of amorphous material is observed. The broader and less intense diffraction peaks attribute to the presence of smaller crystals according to Scherrer law [21]. Presence of amorphous phase is also evident from SEM micrograph (Fig. 2a). The SEM micrograph (Fig. 2a) of the laboratory synthesized catalyst (n-HZSM-5) agrees well to the literature reported [13] SEM micrograph (Fig. 2b). The existing difference between the present and literature reported SEM micrograph (Fig. 2) as well as lesser crystallinity of our laboratory synthesized n-HZSM-5 might be due to difference in synthesis time and temperature condition [15,16]. However, several authors have shown that mainly the greater pore size and high external surface area favour the cat-

Table 3  
Experimental conditions for TGA studies using optimum catalyst percentage

Sample	Nonisothermal experiments			
	Initial mass (mg)	Heating rate (K min <sup>-1</sup> )	Temperature range (K)	$T_{W_0}/T_d/T_m/T_{W_\infty}$ (K)
PP + n-HZSM-5 (50% wt.)	12.78	5	303–873	373.5/413/545.9/874.1
	12.58	10	303–873	373.3/401.6/561.6/874.9
	12.96	15	303–873	373.9/398.6/581.5/875.6
	12.31	20	303–873	373.8/391.3/599.0/877.5
	13.06	25	303–873	373.3/386.3/601.4/877.7

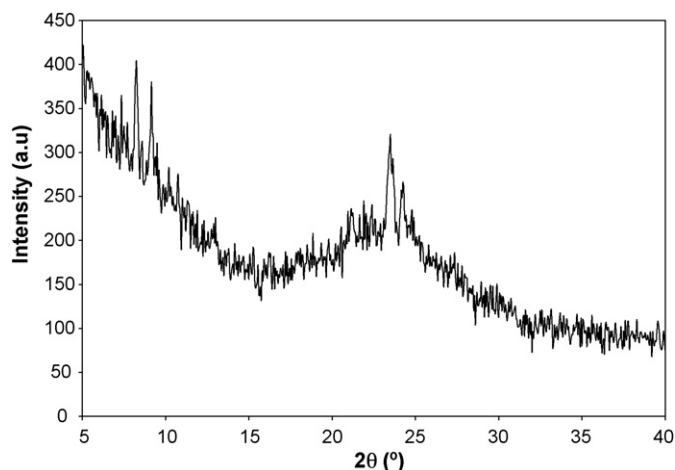


Fig. 1. XRD pattern of n-HZSM-5 catalysts.

alytic activity on degradation of polymers such as LDPE and PP [7,9–11,22–25]. The present n-HZSM-5 catalyst has high external surface area ( $364 \text{ m}^2 \text{ g}^{-1}$ ) due to its nanometric dimensions (Table 4). Particle size distribution analysis using dynamic light scattering, DLS (HORIBA LB-550V, Japan) analyzer with viscometer for the catalyst showed that majority of the particles lie in the range of 50–300 nm. The steep rise in adsorption (Fig. 3) at higher relative pressures ( $P/P^0 > 0.90$ ) is due to the high reported

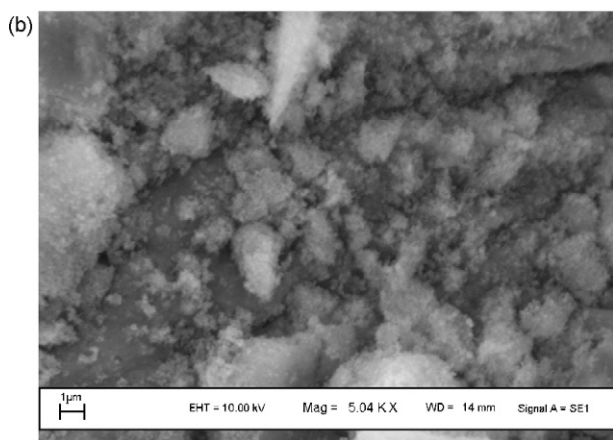
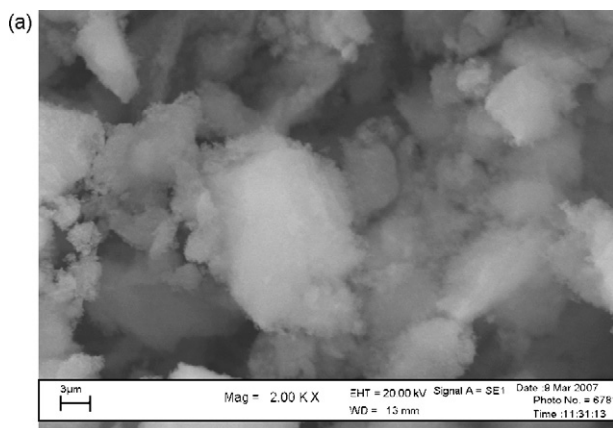


Fig. 2. SEM micrograph of n-HZSM-5: (a) present work and (b) literature work [12].

Table 4  
Textural properties of n-HZSM-5

Sample	n-HZSM-5
BET surface area ( $\text{m}^2 \text{ g}^{-1}$ )	695.58
External surface area (by t-plot surface area) ( $\text{m}^2 \text{ g}^{-1}$ )	364.44
Micropore volume (by t-plot surface area) ( $\text{cm}^3 \text{ g}^{-1}$ )	0.13951
Pore volume (at $P/P^0 = 0.9814$ , adsorption) ( $\text{cm}^3 \text{ g}^{-1}$ )	0.8877

pore volume value of  $0.89 \text{ cm}^3 \text{ g}^{-1}$  at  $P/P^0 = 0.98$ . Thus, the high surface area and pore volume suggests the existence of mesoporosity/macroporosity among the primary nanocrystals formed with the n-HZSM-5 samples [21].

#### 4.2. Noncatalytic and catalytic decomposition

Noncatalytic thermal decomposition of the PP samples was carried out at five different heating rates (5, 10, 15, 20, and  $25 \text{ K min}^{-1}$ ) and the experimental results have been reported in our recent publications [4,19,26]. However, the temperature at which  $\alpha = 0(T_{W_0})$ , the temperature at which decomposition starts and  $\alpha \approx 0.01(T_d)$ , the temperature at which the maximum weight loss rate occurs ( $T_m$ ), and the temperature at the end of the pyrolysis step ( $T_{W_\infty}$ ) are reported in Table 1 for each case of experiments. It was observed that both the thermogravimetric (TG) curves and derivative thermogravimetric (DTG) curves show constant pattern behaviour at different heating rates and higher heating rate finishes the decomposition phenomenon faster [4,19]. The DTG curves were also found to be consisting of single peak that apparently indicates existence of single-step reaction. The constant pattern behaviour is attributed to the fact of similar reaction mechanism, which is the basis of isoconversional (model-free) approach for kinetics analysis [4,27].

Presence of n-HZSM-5 catalyst significantly reduces the  $T_m$  of the PP sample (Fig. 4). The reduction is very significant at lower catalyst compositions and gradually decreases at higher concentrations. It is observed from the figure (Fig. 4) that the optimum catalyst percentage is around 50 wt%, since, after that reduction in  $T_m$  with increase in catalyst percentage is almost

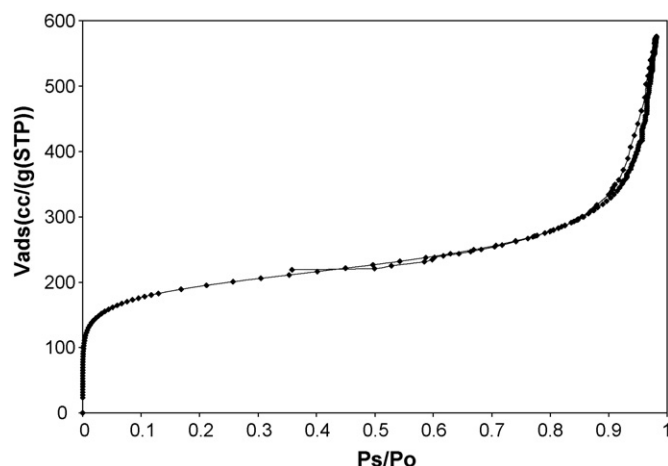


Fig. 3. Nitrogen adsorption isotherm at 77 K of n-HZSM-5 catalysts.

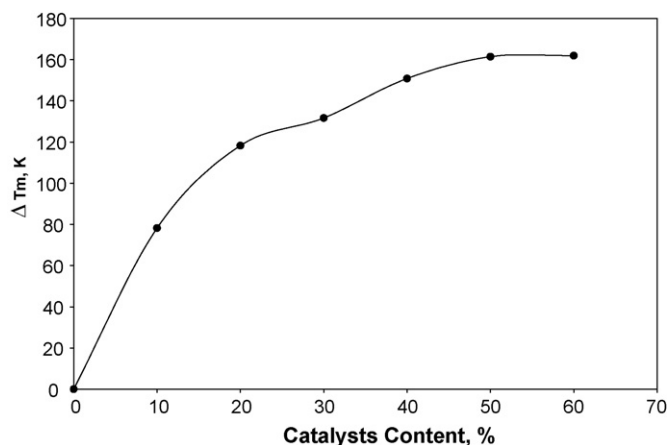


Fig. 4. Effect of catalyst on reduction in maximum decomposition temperature.

negligible. To illustrate quantitatively, it may be seen that for a change of catalyst percentage from 50 to 60 wt%, the further reduction in  $T_m$  is about  $0.5^\circ\text{C}$ , whereas for a change of catalyst percentage from 0 to 10 wt%, 10 to 20, 20 to 30, 30 to 40, and 40 to 50 wt%, the further reduction in  $T_m$  are  $78.3$ ,  $40$ ,  $13.4$ ,  $13.4$ , and  $10.6^\circ\text{C}$ , respectively (Fig. 4). The reduction in maximum decomposition temperature is around  $161^\circ\text{C}$  at 50 wt% catalyst. The catalytic activity of the n-HZSM-5 is due to presence of high external surface area that enhances its cracking activity because the catalyst external acid sites are not sterically hindered for the conversion of the bulky polyolefin molecules [7,10,11], and promotes end-chain scission reactions of the polymers [10]. First chain scissions start on the external surface of the catalyst and then smaller chains can enter into the pores where most of the active sites are located [7].

#### 4.3. Catalytic nonisothermal decomposition at several heating rates

Nonisothermal catalytic decomposition of the PP was carried out at five different heating rates (5, 10, 15, 20, and  $25\text{ K min}^{-1}$ ) with the optimum catalyst percentage of 50 wt%. The temperatures  $T_{W_0}$ ,  $T_d$ ,  $T_m$  and  $T_{W_\infty}$  for the experiments are also reported in the Table 3. Variation of  $\alpha$  with temperature (TG curves) for catalytic (50 wt%) decomposition at different heating rates are reported through Fig. 5. Variations of rate,  $d\alpha/dT$  with temperature (DTG curves) during nonisothermal pyrolysis using catalyst n-HZSM-5 (50 wt%) at different heating rates are reported through Fig. 6. It is again observed from Fig. 5 that like noncatalytic case, the TG curves show constant pattern behaviour indicating existence of similar reaction mechanism and higher heating rate finishes the decomposition phenomenon faster. This is also supported by the almost similar peak height and constant pattern behaviour of the DTG curves (Fig. 6) for the catalytic decomposition of PP. However, it can be observed that at  $5\text{ K min}^{-1}$  heating rate the DTG peak is relatively narrow with higher peak height indicating the fact that at relatively lower heating rate of  $5\text{ K min}^{-1}$  the decomposition takes place in a relatively smaller temperature range. The appearance of the shoulder at relatively higher heating rates of 20 and  $25\text{ K min}^{-1}$ ,

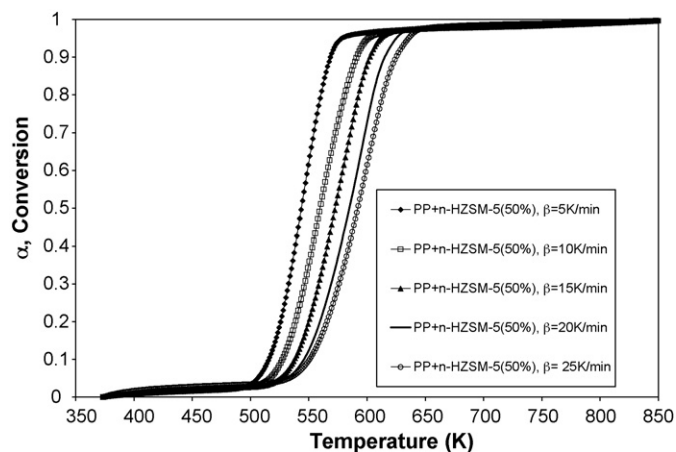


Fig. 5. Variation of conversion ( $\alpha$ ) with temperature during catalytic nonisothermal pyrolysis (50 wt% n-HZSM-5 catalyst) of PP sample.

though insignificant, indicates possible existence of another step in the reaction mechanism, which can be confirmed through further studies on product distribution at different temperatures and at different heating rates.

#### 4.4. Model-free kinetic analysis for PP decomposition

Dependency of  $E_\alpha$  on  $\alpha$  for nonisothermal decomposition of the PP in the present study as well as the literature data is presented through Fig. 7. It is observed from the figure that in case of noncatalytic decomposition of the present PP sample of melt flow index (MFI) 3.0,  $E_\alpha$  is a slowly increasing function of  $\alpha$  in the range ( $0.1 \leq \alpha \leq 0.9$ ). Similar trends are reported by Filho et al. [1] and Peterson et al. [28]. In the present investigation, we used PP sample of MFI 3.0, whereas Filho et al. [1] used PP sample of higher melt flow index 11.5, i.e. of lower molecular weight but with filler calcium carbonate (12 wt%). Peterson et al. [28] used PP sample of average molecular weight (12,000). Therefore, the existing differences in the activation energy might be due to different molecular weights of the PP samples used for the different cases as well as due to the effect of the inorganic

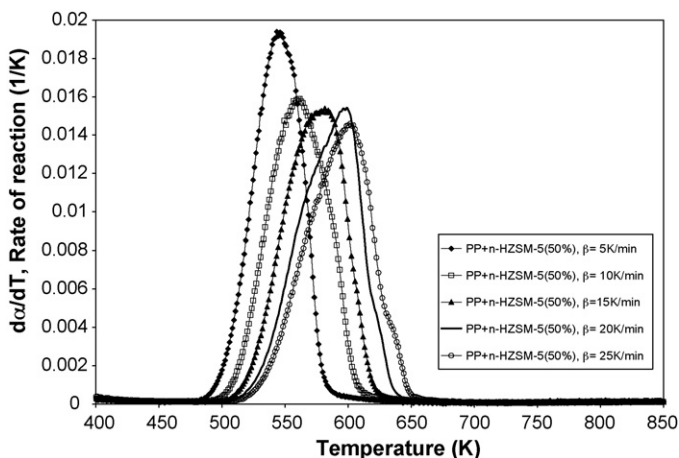


Fig. 6. Variation of rate of decomposition ( $d\alpha/dT$ ) with temperature during catalytic nonisothermal pyrolysis (50 wt% n-HZSM-5 catalyst) of PP sample.

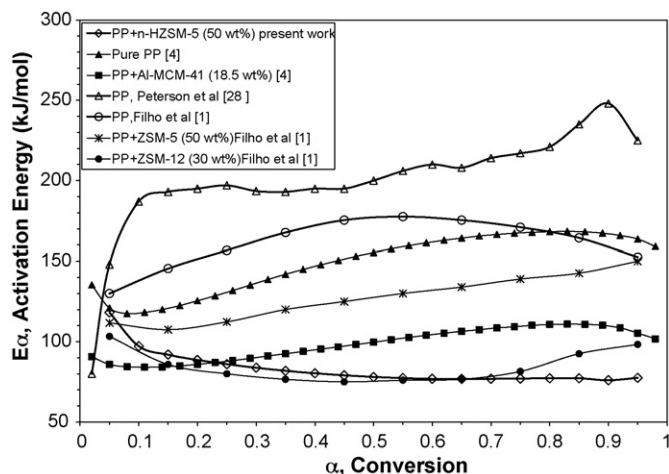


Fig. 7. Dependency of activation energy on conversion of catalytic and noncatalytic nonisothermal decomposition of PP sample (present work and literature reported data).

filler in the PP sample used by Filho et al. [1]. The same is discussed in our recent publication [4].

Fig. 7 also compares the dependency of  $E_\alpha$  on  $\alpha$  for nonisothermal and catalytic decomposition of PP for different catalysts used. It is observed from the figure that for Al-MCM-41 [4] and ZSM-5 [1] catalyzed decomposition,  $E_\alpha$  is a slowly increasing function of  $\alpha$  in the range of  $0.1 \leq \alpha \leq 0.9$ . In case ZSM-12 [1] catalyst,  $E_\alpha$  is a slowly decreasing function of  $\alpha$  for  $\alpha \leq 0.3$ .  $E_\alpha$  is almost constant in the range of  $0.3 \leq \alpha \leq 0.7$  and then slowly increases with  $\alpha$  for  $\alpha \geq 0.3$ . In case of the present catalyst n-HZSM-5,  $E_\alpha$  is a slowly decreasing function of  $\alpha$  for  $\alpha \geq 0.1$ . In general, Fig. 7 suggests that  $E_\alpha$  for catalytic decomposition is much lower than that for noncatalytic one. Exactly similar trends for catalytic (Al-MCM-41 and ZSM-5) and noncatalytic cases for any value of  $\alpha$  further justify the fact that similar reaction mechanism is followed for both the cases of decomposition. Thus, only effect of catalyst is observed in the form of reduction of the temperature and the activation energy [4]. The existing difference between the effects of catalysts Al-MCM-41, ZSM-5 and ZSM-12 is already discussed in our recent publication [4]. Fig. 7 further suggests that ZSM-12 and n-HZSM-5 are better performing than Al-MCM-41 and ZSM-5 catalysts in terms of reduction in activation energy though the catalyst loading is relatively higher than Al-MCM-41. It may further be noted based on Table 2 and Fig. 4 that at 18.5 wt% n-HZSM-5 catalyst loading the reduction in  $T_m$  is about 113 K. But for Al-MCM-41 it was 103 K with the same catalyst loading (which is the optimum catalyst loading for Al-MCM-41) [4]. This again confirms the fact that n-HZSM-5 is better catalyst even at the optimum catalyst loading condition of Al-MCM-41. ZSM-12 and n-HZSM-5 show almost similar effect on the degradation of PP sample up to  $\alpha = 0.7$ . PP has greater cross-sectional area due to the presence of the methyl group that increases certain steric hindrance, which can affect the order of activity of the different catalysts [7,23]. Hence, the catalytic decomposition of PP must start on the external surface of the catalyst and then enter into the pores where they get cracked further leading mainly to the higher olefins and liquid

products [1,7,18,22,24,29]. This is possibly a common phenomenon both for mesoporous and microporous catalysts. Thus, only effect of catalyst is observed in the form of reduction of the temperature and the activation energy at this stage of decomposition. At the later stage of ZSM-12 catalyzed decomposition, the reaction mechanism possibly takes different path for oligomerisation, cyclization, and hydrogen transfer reactions particularly in the micropores [1,22]. The diffusional resistances become predominant for catalysts with comparable pore sizes, i.e. the micropores. Therefore, it is expected that catalyst with wide pore size would give less diffusional resistance and would be more effective towards decomposition of PP. Further, both ZSM-12 and n-HZSM-5 have smaller crystallite size and greater external macropore and mesopore surface, which make the catalysts efficient in the degradation activity for PP.

However after  $\alpha \geq 0.7$  the behaviour is differed markedly. The strong and increasing values of  $E_\alpha$  with  $\alpha$  at the later part of ZSM-12 catalyzed decomposition is just opposite to the trend observed in case of our n-HZSM-5 catalyzed decomposition. This is possibly due to existence of larger external surface in n-HZSM-5 in comparison to ZSM-12. Again, Durmus et al. [7] reported that higher amount of coke deposition occurs over same pore structure with higher the number of acid sites. Si/Al ratio are quite high for both Al-MCM-41 (Si/Al = 35.6) and n-HZSM-5 (Si/Al = 60) catalysts than those of ZSM-5 (Si/Al = 23.7) and ZSM-12 (Si/Al = 29.3) used by Filho et al. [1]. Therefore, the increasing trend of activation energy for both ZSM-5 and ZSM-12 catalysts with similar acidic strength at the later stage of conversion (Fig. 7) might be due to their microporous activity and coke deposition occurring over pore, which is not the case for the mesoporous Al-MCM-41 catalyst and the present n-HZSM-5 catalyst with high external surface area.

## 5. Conclusion

Characterization of nanocrystalline HZSM-5 catalyst as synthesized in the present work indicates existence of amorphous phase with large external surface area. Both thermal and catalytic decomposition of PP sample is studied to understand the effect of n-HZSM-5 catalyst on the decomposition behaviour of PP. Results show that reduction of the maximum decomposition temperature is very sharp at lower catalyst percentage and then change in reduction becomes insignificant at higher catalyst percentage. The optimum catalyst percentage was around 50 wt%, where the reduction in maximum decomposition temperature is about 161 °C. The constant pattern behaviour observed from the TG and DTG curves for the catalyzed decomposition indicates presence of similar reaction mechanism in the decomposition process. The nonlinear Vyazovkin model-free kinetics analysis technique applied to evaluate the quantitative information on variation of  $E_\alpha$  with  $\alpha$  for the PP sample under catalytic nonisothermal condition indicates that  $E_\alpha$  decreases slowly and continuously with  $\alpha$  after  $\alpha \geq 0.1$ . From the comparison of the effects of other catalysts on PP samples, it is found that n-HZSM-5 catalyst is superior to Al-MCM-41 reported by us previously [4] and to ZSM-5 catalyst used by Filho et al. [1] in terms of activation energy,  $E_\alpha$ . But ZSM-12 [1] and the present cata-

lyst, n-HZSM-5 showed almost similar result up to  $\alpha = 0.7$ . The increasing trend of activation energy at higher conversion for both ZSM-5 and ZSM-12 catalysts is possibly due to their microporous activity and coke deposition occurring over pore, which is not the case for the present n-HZSM-5 catalyst with high external surface area. Though 50 wt% catalyst concentration is found to be optimum, catalyst reusability study is very much essential to conclude upon the actual economic optimum.

## References

- [1] J.G.A.P. Filho, E.C. Graciliano, A.O.S. Silva, M.J.B. Souza, A.S. Araujo, *Catal. Today* 107/108 (2005) 507.
- [2] B. Saha, A.K. Maiti, A.K. Ghoshal, *Thermochim. Acta* 444 (2006) 46.
- [3] B. Saha, A.K. Ghoshal, *Thermochim. Acta* 451 (2006) 27.
- [4] B. Saha, A.K. Ghoshal, *Thermochim. Acta* 460 (2007) 77.
- [5] B. Saha, A.K. Ghoshal, *Ind. Eng. Chem. Res.* 46 (2007) 5485.
- [6] P. Carniti, A. Gervasini, *Thermochim. Acta* 379 (2001) 51.
- [7] A. Durmus, S.N. Koc, G.S. Pozan, A. Kasgoz, *Appl. Catal. B* 61 (2005) 316.
- [8] A.S. Araujo, J.V.J. Fernandes, G.J.T. Fernandes, *Thermochim. Acta* 392/393 (2002) 55.
- [9] J. Aguado, D.P. Serrano, G.S. Miguel, J.M. Escola, J.M. Rodríguez, *J. Anal. Appl. Pyrol.* 78 (2007) 153.
- [10] J. Aguado, D.P. Serrano, J.L. Sotelo, R. Van Grieken, J.M. Escola, *Ind. Eng. Chem. Res.* 40 (2001) 5696.
- [11] D.P. Serrano, J. Aguado, J.M. Escola, *Ind. Eng. Chem. Res.* 39 (2000) 1177.
- [12] S. Vyazovkin, D. Dollimore, *J. Chem. Inf. Comput. Sci.* 36 (1996) 42.
- [13] S. Vyazovkin, *Int. J. Chem. Kinet.* 28 (1996) 95.
- [14] S. Vyazovkin, N. Sbirrazzuoli, *Macromol. Rapid Commun.* 27 (2006) 1515.
- [15] R.V. Grieken, J.L. Sotelo, J.M. Menéndez, J.A. Melero, *Micropor. Mesopor. Mater.* 39 (2000) 135.
- [16] R.V. Grieken, J.M. Escola, J. Moreno, R. Rodríguez, *Appl. Catal. A* 305 (2006) 176.
- [17] B. Saha, A.K. Ghoshal, *Chem. Eng. J.* 111 (2005) 39.
- [18] B. Saha, A.K. Ghoshal, *Ind. Eng. Chem. Res.* 45 (2006) 7752.
- [19] B. Saha, A.K. Ghoshal, *Thermochim. Acta* 453 (2007) 120.
- [20] MATLAB® help, Version 7.0.0.19920 (R14), The Math Works, Inc., Natick, MA, 2004.
- [21] D.P. Serrano, J. Aguado, J.M. Escola, J.M. Rodríguez, *J. Anal. Appl. Pyrol.* 74 (2005) 353.
- [22] D.P. Serrano, J. Aguado, J.M. Escola, J.M. Rodríguez, G.S. Miguel, *J. Anal. Appl. Pyrol.* 74 (2005) 370.
- [23] A. Marcilla, M.I. Beltran, R. Navarro, *J. Anal. Appl. Pyrol.* 76 (2006) 222.
- [24] A. Marcilla, A. Gómez-Siurana, D. Berenguer, *Appl. Catal. A* 301 (2006) 222.
- [25] A. Marcilla, A. Gómez-Siurana, F. Valdés, *J. Anal. Appl. Pyrol.* 79 (2007) 433.
- [26] B. Saha, P. Karthik Reddy, A.K. Ghoshal, *Chem. Eng. J.* (2007), doi:10.1016/j.cej.2007.05.024.
- [27] S. Vyazovkin, C.A. Wight, *Thermochim. Acta* 340/341 (1999) 53.
- [28] J.D. Peterson, S. Vyazovkin, C.A. Wight, *Macromol. Chem. Phys.* 202 (2001) 775.
- [29] Y.-H. Lin, H.-Y. Yen, *Polym. Degrad. Stab.* 89 (2005) 101.